LA-8105-MS
Informal Report

The Simulated-Photograph Technique as a Tool for the Study of Visibility Impairment

University of California

LOS ALAMOS SCIENTIFIC LABORATORY
Post Office Box 1663 Los Alamos, New Mexico 87545

This report was not edited by the Technical Information staff.

This work was supported by the US Department of Energy, Office of Technology Impacts, Policy Analysis Division, and the Office of Coal and Electrical Systems Policy, and the US Department of the Interior.

UNITED STATES
DEPARTMENT OF ENERGY
CONTRACT W-7405-ENG. 36

LA-8105-MS
Informal Report
UC-11
Issued: October 1979

The Simulated-Photograph Technique as a Tool for the Study of Visibility Impairment

Michael D. Williams
Evelyn Treiman*
Mona Wecksung

*Department of Biology, University of Montana, Missoula, MT 59812.

THE SIMULATED-PHOTOGRAPH TECHNIQUE AS A TOOL FOR THE STUDY OF VISIBILITY IMPAIRMENT

by

Michael D. Williams, Evelyn Treiman, and Mona Wecksung

ABSTRACT

With the 1977 Clean Air Act amendment, visibility impacts of anthropogenic emissions in national parks and wilderness areas assume increased importance. Existing sources that produce visibility effects may be required to clean up, and proposed new sources may be faced with new siting and emission control constraints. Consequently it is important to develop visibility models that can translate emissions, meteorology, and topography into visibility impacts. Furthermore, because many of the key decision makers identified in the Act are resource managers without training in air dispersion or radiative transfer, it is important to produce visibility models with easily understood outputs.

To meet these needs Los Alamos Scientific Laboratory (LASL) investigators have developed the LASL visibility model and the simulated-photograph technique (SPT). The SPT transforms the results of visibility models into pictures that display the modification of a scene by air contaminants, thus producing outputs understandable to untrained persons. The SPT technique can be used to compare various models, identify important variables, and aid decision makers.

The LASL visibility model consists of several modules that compute light scattering by particles, air dispersion, and radiation transfer through a pollutant cloud. The features of the model, its limitations, and its uses along with those of the SPT are described.

I. INTRODUCTION

This report describes the use of the simulated-photograph technique (SPT) developed for the Department of Energy by the Los Alamos Scientific Laboratory (LASL) to determine visibility impairment; it presents several SPT applications. With passage of the 1977 Clean Air Act amendments, particularly sections 169A and 165(d), protection against visibility impairment in mandatory Class I Federal areas (such as national parks and wilderness areas) has been established as a national goal. Ultimately, visibility also may be protected by emission restrictions on new and existing individual pollution sources. In this context, it is extremely important to develop an effective decision-making tool that can be used by regulatory agencies to assess potential visibility impairment associated with various combinations of source emission characteristics and meteorological conditions.

There are two general approaches to assessing visibility impairment. The first is to calculate quantities to be used as appropriate visibility indices; the second involves a photograph that indicates the degree of visibility impairment. The visibility measurement indices suggested for the first approach include Commission Internationale de l'Eclairage (CIE) ΔE values, blue/red ratio, plume-to-horizon brightness ratio, bscat, and b extinction. These indices are described in detail in the literature.[1]

Any approach that attempts to characterize visibility impairment by visibility indices has two major difficulties. First, because the above indices are not meaningful to untrained persons, it is difficult for them to determine the visibility level at which impairment is significant. Because the human eye-brain system responds primarily to abrupt changes in color or intensity, in plume blight situations a plume having a sharp boundary is much more visible than a plume having a very diffuse boundary. Second, it is difficult to represent actual overall visibility impairment with only a few visibility indices.

Two techniques, which produce actual pictures as model outputs, have been developed to correct the deficiencies of visibility indices alone. In the first technique, produced by Systems Applications, Inc. (SAI), a code computes the sky color, which then is painted in by a commercial artist. The second technique is the SPT discussed below.

In the SPT, a photographic slide is taken of a scene in the area of interest. The slide is analyzed by a microdensitometer, which measures the

optical density* of a very small area of the film for each of the colors--blue, green, and red. When this information is displayed on a color TV screen, the original picture can be seen in color and can be photographed.

The microdensitometer analysis information is stored on magnetic tape. Next, computer programs** calculate the potential concentration of pollutants between the observer and the scene as a consequence of the siting and operation of one or more new or modified sources. Specifically, pollutants reduce the light that is transmitted through the air from some distant point and increase the light that is reflected toward the observer by small particles in the air. The pollution is displayed on the screen to provide a new color picture representing the potential visibility impairment caused by the sources' emissions. This technique also can be used to ascertain the amount of visibility impairment caused by varying the degree of pollution control to be applied to a proposed or existing source. With this technique, the public, decision makers, regulatory agencies, and courts can be provided with simulated photographs of the potential visibility impairment resulting from various pollution control scenarios. The benefits in visibility improvement can be assessed directly by photographic display and then can be weighed against the cost of control.

Visibility indices are apt to be more useful where air pollution is relatively uniform (haze) than where plume blight is a problem. In the case of haze, only one or two parameters may be enough to characterize a scene so that the entire picture need not be generated for each scenario. In the case of plume blight, where there is an obvious plume in which pollutant concentrations vary greatly from point to point, visibility indices are apt to be unsatisfactory. In this instance, the more detailed information provided by the SPT is beneficial to identify the potential visual result. A great deal of information is necessary to characterize a plume blight adequately; here, a picture is the most convenient form in which to communicate this information.

---

*The optical density determines the light transmission of a slide and thus determines the brightness of the screen upon which the slide is projected. The microdensitometer divides the slide into many small areas and measures the optical density of each area.

**These programs compute the manner in which pollutants are diluted as they mix with clean air and are transported by the wind.

The SPT is not limited to one air quality modeling system. It can be used on any system that can provide light transmissions and the additional light scattering associated with pollutants. It also can be used on systems that provide only light intensities but with a possible loss in accuracy in the depiction of the landscape behind the pollution.

II. FACTORS AFFECTING SPT ACCURACY

The SPT can be used for visibility model validation and development, comparison of visibility models, policy evaluation, and as a regulatory tool for decision makers. To validate models simulated pictures can be made using various predictive models for circumstances under which actual photographs have been made. Comparison of the simulated and actual photographs permits a rough estimate of a model's validity.

A simulated photograph, prepared using the SPT LASL visibility model, is compared with an actual photograph of a smoke plume. (See Figs. 1-3, the validation slides.) The resulting photograph, together with a photograph of the color TV screen upon which the information is displayed and the original photograph of the actual plume, are described in Appendix A. Although the simulated photograph was produced using data from the LASL visibility model, other simulated photographs can be produced by other visibility models. Photographs of this nature can be used to compare the results of various predictive models, and model parameters that lead to discernible differences can be identified easily.

A principal advantage of the SPT is in the area of policy evaluation. In other visibility modeling predictive techniques, the significance of changes in the value of indices must be assessed numerically. The SPT produces a comparable set of "before" and "after" photographs.

One difficulty with the SPT that is yet to be resolved is a proper incorporation of the pyschophysics of the visibility problem. Manufacturers of color film and color televisions have long appreciated the fact that adequate reproduction of color images requires sophisticated understanding and treatment of the human visual system. For example, photographs which transform outside scene brightnesses into the proper mix of brightnesses on a slide or print will appear washed out. Film manufacturers have long recognized this fact and therefore have developed films that increase the differences in brightnesses over those in the original scene. This is

necessary because of differences in the way in which the original scene, viewed outdoors with the eye adapted to high light levels and the slide or print, viewed indoor with the eye adapted to low light levels, is perceived. Furthermore, the photograph usually is illuminated with a much different color temperature light than is the outdoor scene. Currently the SPT involves photographing a TV screen with filters and film appropriate for daylight use, which may not properly consider the pyschophysics of visibility impairment. A system is being developed that should permit the construction of simulated photographs that are consistent with normal photographic reproduction of outdoor scenes.

In addition to the psychophysics problems discussed above, there are other uncertainties associated with each of the following SPT components. (1) the input parameter estimation, (2) the modeling of pollutant dispersion and radiative transfer, and (3) the representation on the TV screen and on film of the brightnesses of individual picture elements. There are four principal sources for (3): (1) the representation of the original scene by the camera-film system, (2) the extraction of data from the film by the microdensitometer, (3) the representation of the extracted data by the color TV system, and (4) the representation of the color TV picture by the camera-film system.

The camera-film system represents the contrast between various photographic elements by the optical densities of three emulsions. (Emulsions are light-sensitive coatings in a thin gelatin layer on film). The accuracy of the representation depends upon the exposure of individual elements; poor representations occur if the element is either significantly underexposed or overexposed. Furthermore, slight differences in the response of one emulsion vis-a-vis another emulsion translate into noticeable changes in color. To some extent, compensation can be made for the distortions produced by the film. The photographs produced for this report used published film characteristics. However, films vary slightly from one batch to another so that the characteristics of any specific batch probably will differ slightly from the published characteristics. The film grain size also limits the detail that can be depicted by the film. No adjustment for film characteristics was made in the validation photographs, because the film characteristics were not available in this instance.

The camera-lens system produces additional distortions associated with vignetting, the process by which the center of the picture may receive more light than its sides, and with reflected light from lens surfaces and dust on lenses.

Measuring optical densities with a microdensitometer involves loss of detail because, at present, only 340 lines of 512 points each are used to represent the entire picture. More detail could be obtained by using more points, at the expense of increased computer time. Furthermore, slight changes in color are possible because the filters on the microdensitometer for one color light will transmit some of the other colors.

The color TV also may slightly distort the input used to produce the pictures. However, there are devices that can write digital information onto film without using a color TV.

The camera-film system introduces similar aberrations to camera-lens aberrations. The use of other devices could eliminate the camera from the system, but the film would remain. However, the digital data can be predistorted to compensate partially for the film aberrations, although doubtless some errors would remain.

The model's output is sensitive to the input data and, in some cases, there have not been enough measurements to reduce the uncertainty. In this context, key variables that can introduce uncertainty are the size distribution of secondary aerosols (sulfates and nitrates), the rates of conversion of secondary aerosols from primary contaminants, the rates of formation of nitrogen dioxide from nitric oxide, the size distribution of primary contaminants, and the meteorological variables that describe the contaminant dispersion.

III. SPT APPLICATIONS

Several photographs, which display simulated power plant smoke plumes under various conditions, illustrate the SPT capabilities. Figures 4-18 deal with a plume blight situation in which the plume can be readily associated with a particular source. Figure 4, the base case from which the input parameters are varied, shows a smoke plume from a 2000-MW coal fired plant as seen during low to moderate wind speeds and stable atmospheric conditions. Further details of the source evaluation are found in Appendix A. The parameter range includes plant size; sun scattering angle; meteorological conditions; plume orientation angle; distance from the observer to the plume;

topography; rate of conversion of nitrogen oxides to nitrogen dioxide, rate of conversion of nitrogen oxides to particulate nitrate; rate of conversion of sulfur dioxide to sulfate, size distribution of secondary particules; background visual range; relative humidity; and nitrogen oxide, sulfur dioxide, and fly ash emissions. Some variations are discussed below.

A. Impact of Plant Size

Figure 5 shows the plume from a 1000-MW plant, and Fig. 6 shows the plume from a 500-MW plant. It is evident that overall plant size is a key variable in visibility effects.

B. Impact of Atmospheric Stability

Figures 7 and 8 show how changes in atmospheric stability affect visibility impairment predictions. Figure 7 illustrates plume behavior during neutral (D) conditions according to Turner* classification. Figure 8 illustrates plume behavior during slightly stable (Turner E) conditions. The base case used stable conditions according to the Tennessee Valley Authority (TVA)** classification. Within current knowledge, either the TVA stable or the Turner slightly stable (E) classification might be applied to atmospheres having the same measured meteorological characteristics. In some cases it is difficult to distinguish between slightly stable (Turner E) and neutral (Turner D) conditions. These photographs indicate that the appearance of the plume is affected greatly by atmospheric dispersion characteristics.

C. Impact of Particulate and Nitrogen Oxide Emissions

Figures 9 and 10 show the effect of changes in emission parameters. Figure 9 shows a plume with fly ash emissions increased threefold from the base case. In this instance, additional light scattering by particulates masks the browning effect of light absorption by nitrogen dioxide. In Fig. 10, nitrogen oxide emissions have been increased by 50%. These photographs, compared to the base case, show that the magnitude of nitrogen oxide emissions is very important to the appearance of a plume.

---

*The Turner stability categorization classifies atmospheric stability with the letters A through F, depending upon time of day, wind speed, and cloud cover; F is the most stable. Parameters describe the depth and width of the plume as a function of distance for each category.[2]

**The TVA has published a slightly different set of stability parameters based on their experience with power plant plumes.[3]

D. Impact of Viewing Angle and Time of Day

Geometry also can be important in the perception of a scene. Figure 11 depicts the base case at a time of the day when the observer is looking toward the sun. The plume appears much lighter on the left—nearer the sun—than on the right, because more light is scattered at small scattering angles. In this case, scattering plays a key role.

E. Impact of Background Factors

The context in which the plume is seen is also important. Figure 12 illustrates the base case with the relative humidity increased from 30% to 80%. The picture appears much hazier and the plume is much less obvious than in the base case. Figure 13 depicts the plume as it would be seen in the eastern part of the United States where the background particulate loading is much higher than in the West. In this instance, the background haze makes the plume indistinguishable.

F. Impact of Topography

The background against which the plume is observed is a key variable. Figure 14 depicts the plume against a dark background. In this case, the plume is much less obvious because it is primarly an absorbing plume.

G. Impact of Plume-Observer Geometry

Important factors in the observer's perception include the distance between the observer and the plume and the direction the plume travels relative to the viewing direction. Figure 15 illustrates the picture as seen by an observer much closer to the plume centerline than the observer in the base case. Here, the plume appears to spread over a large area with diffuse boundaries.

Figure 16 shows a plume traveling toward the observer.

Another important factor is the manner in which the brightness varies with the angle in a given scene. In this context, two similar pictures with plumes having similar numerical indices (Figs. 4 and 15) are much different in appearance. In Fig. 4, the plume is a narrow strip across the picture; in Fig. 15, most of the sky is obscured by the plume. Because the brightness changes were gradual in Fig. 15, the plume is much less apparent than in Fig. 4.

H. Impact of Size Distribution and Sulfur Dioxide Emission Rate

Figure 17 illustrates the plume from a 2000-MW plant when sulfur dioxide emissions are increased threefold from the base case. In this instance, there

is little change in appearance. In Fig. 18, however, both the sulfur dioxide emissions and the sulfate particulate size have been increased. For higher emissions than in the base case, the secondary particle size distribution is an important variable.

I. Simulation of Haze

In a similar fashion, a uniform haze can be simulated with the SPT. Figures 19-25 have been produced to illustrate this capability. Figure 19 is a copy of an actual photograph on a relatively clear day that might correspond to a background concentration of 0.6 $\mu g/m^3$ of sulfate in combination with other particulates. Figure 20 is the computer reconstruction of Fig. 19. Figure 21 represents the same scene on a somewhat hazier day that might correspond to 5 $\mu g/m^3$ of particulate sulfate. Figure 22 represents the same scene with haze levels associated with 26 $\mu g/m^3$ of sulfate. In this instance the terrain is 13 km from the observer, and the background visual range is 23 km.

Figure 23 represents the original scene with the relative humidity increased from 30% to 60%, and Fig. 24 represents the same scene with the relative humidity increased to 80%. Figure 25 depicts 60% relative humidity coupled with 26 $\mu g/m^3$ of particulate sulfate. It is evident that relative humidity is an important factor in the appearance of regional haze.

Other cases and their associated photographs are described in Appendix A.

IV. EQUIPMENT, TIME, AND COST REQUIREMENTS FOR THE SPT

Key facilities required to produce simulated photographs include a color microdensitometer and a color video display unit, such as a comtal. The microdensitometer measures the light transmission through a very small portion of the film, and the comtal is a color TV set that displays digital data. In addition, computer software is required to permit modification of the digitized data. All this equipment is available at several image-processing institutes, such as the one at the University of Southern California. In addition to the image-processing equipment, computing facilities are also required. At LASL, the entire system consists of a comtal display, a PDP 11-40 computer, a microdensitometer, and a CDC-7600 computer.

Approximately 6 man-hours are needed to produce one picture. However, the per-picture time probably could be decreased if more than one picture were to be made. Much of the 6 hours, which includes starting from scratch on a

single picture, is not used fully, but instead is spent waiting for machine response, tape mounting, etc.

As the technique is used now, it is limited primarily by the need to represent a scene by a combination of three colors. In this sense, the situation is similar to photographs (three emulsions) or color television. Other techniques might be developed to relax this limitation somewhat, but their development would take a year or more and probably is not justified in view of the wide applications of color photographs, which have the same limitations.

Both the technical aspects of the SPT and the simulations used in this chapter are described in technical detail in Appendixes A and B.

V. SUMMARY

A visibility modeling capability would be helpful to evaluate progress toward the national goal of protection of visibility in mandatory Class I areas, as required by the Clean Air Act amendments of 1977. However, two major difficulties must be overcome to obtain the requisite modeling capability. First, a model must be developed which can provide sufficient richness of detail that the full range of subtleties associated with visibility impairment can be assessed. Second, the model output must be in a form that can be made meaningful to the lay audience, scientist, and decision maker alike.

Two visibility impairment situations need to be addressed. The first is regional haze, in which the atmosphere is relatively uniformly degraded with no obvious changes in light-scattering or -absorbing materials. The second, called plume blight, involves an apparent plume that can be traced to one or more specific sources. In the context of plume blight, the perceived effect of the plume depends upon a wealth of detail that probably cannot be represented by any limited form of numerical outputs. In this circumstance, the only satisfactory representation is probably a picture.

To date, two systems, both providing pictures as a final output, have been used to measure visibility impairment. One, the SPT developed for DOE at LASL, produces a photograph that has been modified in accordance with predicted changes in light pattern associated with pollutants. The other, produced by SAI, involves calculating the sky colors and then having a commercial artist paint in the calculated colors. One difficulty of the SAI system is that only the sky is represented accurately. For example, the SAI

system does not provide a good representation of plumes that pass in front of land forms. The SPT does not have this limitation.

Several possible applications of the SPT are related to identification of visibility impairment. It can be used for visibility model validation; development and comparison; policy evaluation; and as a regulatory tool for decision makers. In this report, several examples illustrate the technique's capabilities. The fully apparent ability of the SPT to represent the richness of detail in a scene is much more important in plume blight cases than for haze.

For regional haze cases, SPT is useful primarily because it translates indices such as visual range into a picture that is immediately meaningful to the untrained observer. However, once a few pictures have been prepared, the numerical indices probably can be related to pictures (real or simulated), and the continued use of the SPT for haze situations may not be needed for each case.

The SPT is a regulatory tool, which can be used in a variety of ways to assist in ascertaining progress towards visibility goals. We hope that other air quality experts will carefully review the SPT merits, both for ascertaining visibility impairment and as a regulatory tool to monitor progress towards the visibility goals as established by Congress.

SPT weaknesses include the computer time required and other special facilities needed to produce output. In addition, the need to represent a scene by only three sets of colors is a disadvantage. Furthermore, there are many opportunities to introduce uncertainty into the final output.

REFERENCES

1. Douglas A. Latimer, Robert W. Bergstrom, Stanley R. Hayes, Mei-Kao Liu, John H. Seinfeld, Gary Z. Whitten, Michael A. Wojcik, and Martin J. Hillyer, "The Development of Mathematical Models for the Prediction of Anthropogenic Visibility Impairment," Environmental Protection Agency report EF78-63AR (September 1978).

2. D. B. Turner, Workbook of Atmospheric Dispersion Estimates, U. S. Dept. of Health, Education and Welfare, p. 36, revised 1969.

3. T. L. Montgomery, W. B. Norris, F. W. Thomas, and S. B. Carpenter, "A Simplified Technique used to Evaluate Atmospheric Dispersion of Emissions from Large Power Plants," J. Air Pollut. Contr. Ass., 23, 328-394 (1973).

FIG. 1. ACTUAL PHOTOGRAPH (V-1) OF THE PLUME FROM A 1500-MW COAL-FIRED POWER PLANT.

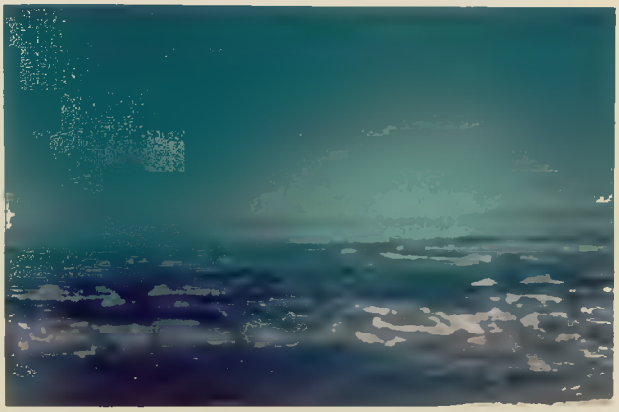

FIG. 2. THIS COMPUTER VERSION (V-2) OF THE SCENE IN FIG. 1 INCLUDES NO CORRECTION FOR FILM CHARACTERISTICS BECAUSE THE ORIGINAL USED AN OUTDATED FILM. FIGURES 20 AND 21 PROVIDE A BETTER COMPARISON.

FIG. 3. SIMULATED PLUME (V-3) FOR THE CASE REPRESENTED IN FIG. 2.

FIG. 4. SIMULATED BASE CASE (B-1) DEPICTING THE PLUME FROM A HYPOTHETICAL 2000-MW PLANT.

FIG. 5. SIMULATED PLUME (B-2) FROM A 1000-MW PLANT.

FIG. 6. SIMULATED PLUME (B-3) FROM A 500-MW PLANT.

FIG. 7. SIMULATED PLUME (B-10) DURING NEUTRAL ATMOSPHERIC CONDITIONS (BASE CASE DEPICTS STABLE CONDITIONS).

FIG. 8. SIMULATED PLUME (B-16) DURING TURNER E STABLE CONDITIONS (BASE CASE IS 0.5 LBS/MMBTU).

FIG. 9. SIMULATED PLUME (B-7) WITH FLY ASH EMISSIONS INCREASED THREEFOLD OVER THE BASE CASE (0.09 LBS/MMBTU VS 0.03 LBS/MMBTU IN THE BASE CASE).

FIG. 10. SIMULATED PLUME (B-17) WITH NOx EMISSIONS REDUCED TO 0.25 LBS/MMBTU (BASE CASE IS 0.5 LBS/MMBTU).

FIG. 11. SIMULATED PLUME (B-9) WITH OBSERVER LOOKING MORE NEARLY TOWARD THE SUN (SCATTERING ANGLE IS 21^0 VS 79^0 FOR THE BASE CASE).

FIG. 12. SIMULATED PLUME (B-15) WITH THE RELATIVE HUMIDITY INCREASED FROM 30% TO 80%.

FIG. 13. SIMULATED PLUME (B-14) IN A HAZY BACKGROUND (126 $\mu G/M^3$ OF PARTICULATE SULFATE VS 0.5 $\mu G/M^3$ IN THE BASE CASE).

FIG. 14. SIMULATED PLUME (B-12) AGAINST A MOUNTAIN BACKGROUND (BASE CASE DEPICTS THE PLUME AGAINST A SKY BACKGROUND).

FIG. 15. SIMULATED PLUME (B-11) WITH THE OBSERVER CLOSER TO THE PLUME (3 KM INSTEAD OF 10 KM IN THE BASE CASE) AND THE PLUME TRAVEL NORMAL TO THE LINE OF SIGHT (ORIENTATION ANGLE FOR THE BASE CASE IS 120^{0} RATHER THAN 90^{0}).

FIG. 16. SIMULATED PLUME (B-13) TRAVELING MORE NEARLY TOWARD THE OBSERVER (ORIENTATION ANGLE IS 165^{0} WHILE THE BASE CASE IS 120^{0}).

FIG. 17. SIMULATED PLUME (B-4) FROM A 2000-MW PLANT WITH SO_2 EMISSIONS INCREASED THREEFOLD OVER THE BASE CASE (0.6 LBS/MMBTU VS 0.2 LBS/MMBTU.

FIG. 18. SIMULATED PLUME (B-6) WITH SO_2 EMISSIONS INCREASED THREEFOLD OVER THE BASE CASE AND INCREASED SULFATE PARTICULATE SIZE (0.2 μMMD VS 0.08 μMMD IN THE BASE CASE).

FIG. 19. PHOTOGRAPH (A-1) OF THE ORIGINAL SCENE USED IN THE SIMULATIONS.

FIG. 20. COMPUTER RECONSTRUCTION (H-2) OF THE ORIGINAL SLIDE.

FIG. 21. SIMULATED HAZE (H-3) WITH 5 $\mu G/M^3$ OF PARTICULATE SULFATE CORRESPONDING TO VISUAL (BASE CASE EQUALS RANGE OF 90 KM 0.5 $\mu G/M^3$).

FIG. 22. SIMULATED HAZE (H-4) WITH 26 $\mu G/M^3$ OF PARTICULATE SULFATE CORRESPONDING TO A VISUAL RANGE OF 22 KM (BASE CASE EQUALS 0.5 $\mu G/M^3$).

FIG. 23. SIMULATED HAZE (H-5) WITH THE RELATIVE HUMIDITY INCREASED TO 60% (BASE CASE HAS 30% RELATIVE HUMIDITY).

FIG. 24. SIMULATED HAZE (H-6) WITH THE RELATIVE HUMIDITY INCREASED TO 80% (BASE CASE HAS 30% RELATIVE HUMIDITY).

FIG. 25. SIMULATED HAZE (H-7) WITH 26 $\mu G/M^3$ OF PARTICULATE SULFATE IN CONJUNCTION WITH 60% RELATIVE HUMIDITY (BASE CASE HAS 0.5 $\mu G/M^3$ OF PARTICULATES AND 30% RELATIVE HUMIDITY).

APPENDIX A

TECHNICAL DESCRIPTION OF THE SPT FOR SELECTED CASE STUDIES

The base case was chosen using a 2000-MW coal-fired plant emitting pollutants at a rate equivalent to recently proposed NSPS for a subbituminous coal-fired power plant.[1] The proposed emission standards include 85% control of sulfur dioxide and restriction of fly ash emissions and nitrogen oxide emissions to 0.03 lbs/MMBTU and 0.5 lbs/MMBTU, respectively. The plant was assumed to be located 30 km from the observer with a wind direction such as to bring the centerline of the plume to 10 km from the observer at the center of the observer's field of view. The plant was assumed to have an electrostatic precipitator to control fly ash emissions and a sulfur dioxide scrubber. Nitrogen oxide controls are inherent in the boiler design. The wind direction was assumed to be inclined slightly toward the observer so that the angle between the observer's line of sight and the plume travel was 120° at the center of the observer's field of vision. Figure A-1 depicts the geometry for this situation, and Fig. A-2 depicts the geometry for validation case photographs.

The wind speed chosen for the base case was 3 m/s with an atmospheric stability of TVA stable, which is nearly identical to Turner F stable. Stack height was 183 m and plume rise conditions corresponded to 500-MW units, all

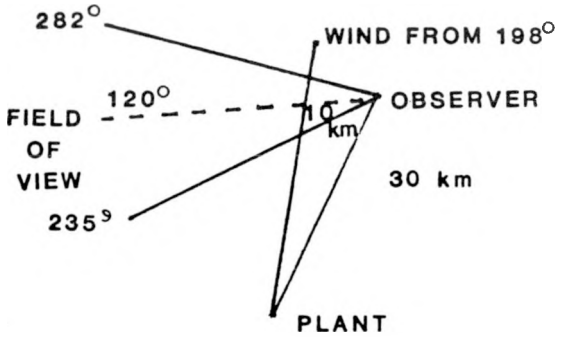

Fig. A-1.
Source-observer geometry for validation case photographs V-1 through V-3 (Figs. 1-3).

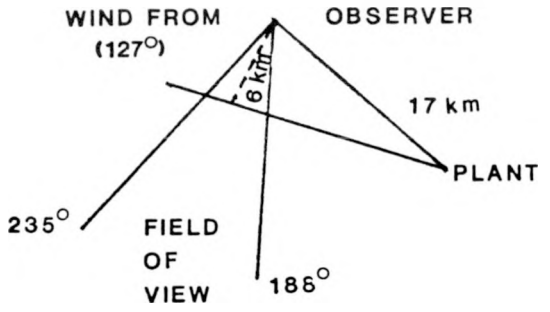

Fig. A-2.
Source-observer geometry for the base case blight simulation.

fully scrubbed. The background visual range corresponded to 250 km for a 5500-A wavelength. This value was chosen because it is approximately the value deduced by turbidity measurements made on the day the original photographs were taken.

The half-life of sulfur-dioxide-to-sulfate conversion was assumed to be 96 hours, whereas the half-life for nitrogen-oxide-to-particulate-nitrate conversion was assumed to be 46 hours. The half-life for conversion of nitric oxide to nitrogen dioxide was taken as 2.8 hours, which is consistent with measurements taken in the Southwest during stable conditions.[2] However, the dispersion model permits a maximum conversion equal to the background ozone plus 35% of the nitrogen oxide. Thus, if the nitrogen oxide concentration were 0.15 ppm and the background ozone level were 0.05 ppm, the maximum nitrogen dioxide concentration would be 0.085 ppm.

The size distribution for sulfate and nitrate particles was based on measurements near the Four Corners power plant in northwestern New Mexico.[3] These values suggest that the sulfates and nitrates are relatively fine, 0.08-micron MMD, and are generally smaller than the optimum size for light scattering. These very fine sulfates presumably occur only during the first few tens of kilometers of travel on days with low relative humidity.

For fly ash, a particulate size distribution equivalent to that measured by Lawrence Livermore Laboratory investigators[4] on a plant fitted with 99.7% effective electrostatic precipitators was used. This results in somewhat less light scattering than would be expected from an equally efficient particulate scrubber because the particles are slightly larger (1.6-micron MMD) than the optimum size for light scattering.

Parameters including the mie scattering and Rayleigh scattering optical depths are taken from McClatchey et al.[5] The optical depths of the lowest six layers of the background atmosphere are adjusted to give a turbidity equal to that measured on the day the photograph was taken. Table A-I summarizes the base case parameters.

The base case photograph was taken at Bandelier National Monument, looking west-southwest across the monument at noon MST on October 26, 1978. The scattering angle for this situation is 79^{o}.

In the plume blight examples, a number of variables were considered. The variables examined were sun angle, distance to the plume, background visual range, plume orientation, topography, atmospheric stability and dispersion,

wind speed, relative humidity, plant size, particulate emission rate, nitrogen dioxide emission rate, and nitrogen oxide emission rate. Table A-II lists the cases and their associated parameter variations.

This range of parameters was chosen to reflect important differences in visibility that normally would be encountered. For example, the scattering angle ranges from 21^{o} to 79^{o}, calculated for the direction of the center of the observer's field of vision. The full range is somewhat greater than these values because the observer's viewing direction can vary by as much as 23^{o} to either the right or the left. The photograph B-9 (Fig. 11), with a 21^{o} scattering angle is about as close to full forward scattering as one gets without the sun actually being in the picture.

The topography differences were chosen because they were expected to highlight some of the features that might alter the plume's appearance. The

TABLE A-I

BASE CASE PARAMETERS

Parameter	Description
Sun angle	Scattering angle = 79^{o}
plume distance	d = 10 km in field-of-vision center
Plume orientation	120^{o} angle between the viewing direction and plume travel
Topography	mixed background mountains (13 km distant) and sky
Stability and dispersion	TVA slightly stable; Turner stability F
Wind speed	3 m/s
Relative humidity	30%
Background visual range	250 km for 5500 A
Fly ash emission rate	0.03 lbs/MMBTU; 74 g/s
Plant size	2000 MW
SO_2 emission rate	0.2 lbs/MMBTU; - 494 g/s
NO_x emission rate	0.5 lbs/MMBTU; - 1236 g/s
SO_2 to SO_4 conversion rate	96-hour half-life; 0.7%/hour
NO_x to NO_3 conversion rate	46-hour half-life; - 1.5%/hour
NO_x to NO_2 conversion rate	2.8-hour half-life; 25%/hour
Fly ash size distribution	E.S.P. of 99.7% efficiency; MMD 1.6 microns
Secondary particulate size distribution (NO_3, SO_4)	Four Corners, MMD 0.08 microns

TABLE A-II

PARAMETER VARIATIONS

Slide Photograph	Parameter
B-1	Base case (simulated photograph)
B-2	Plant size = 1000 MW
B-3	Plant size = 500 MW
B-4	SO_2 emissions rate 0.6 lbs/MMBTU
B-5	SO_2 emission rate 1.2 lbs/MMBTU
B-6	SO_2 emission rate 0.6 lbs/MMBTU and SO_4 mass median diameter 0.2 microns
B-7	Fly ash emission rate 0.09 lbs/MMBTU
B-8	NO_x emission rate 0.7 lbs/MMBTU
B-9	Sun angle; scattering angle = 21
B-10	Atmospheric dispersion Turner D wind speed 5 m/s
B-11	Plume distance 3 km; orientation angle 90°
B-12	Mountain background
B-13	Orientation angle 165°
B-14	Background visual range 22 km
B-15	Relative humdity 80%
B-16	Atmospheric dispersion Turner E stable
B-17	NO_x emission rate 0.25 lbs/MMBTU
B-18	Sun angle; scattering angle 135
B-19	Wind speed 5 m/s
B-20	Dispersion Turner C, mining height 1000 m
B-21	Dispersion Turner C; mining height 3000 m
B-22	Plume distance 3 km; topography red rock
B-23	Plume distance 25 km
B-24	Orientation angle 150°
B-25	Topography flat land and sky
B-26	NO_x-to-NO_3 conversion half-life 20 hours
B-27	NO_x-to NO_3 conversion half-life 200 hours
B-28	SO_2-to-SO_4 half-life 64 hours
B-29	SO_2-to-SO_2 half-life 32 hours
B-30	Secondary particles size (NO_3,SO_4) 0.2 microns MMD
B-31	Secondary particles size (NO_3,SO_4) 0.4 microns MMD
B-32	Fly ash emission rate 0.01 lbs/MMBTU
B-33	NO_x-to-NO_2 conversion half-life 1.0 hours
B-34	NO_x to NO_2 conversion half-life 5.0 hours
B-35	Background visual range 90 km
B-36	Relative humidity 60%

mountain background in photograph B-12 (Fig. 14) would definitely deemphasize the effects of nitrogen oxide absorption that are apparent when the plume is seen against the sky. The range of meteorological conditions chosen represents the range of conditions under which the plume could be expected to be visible. If cases depicting Turner A or B stability with unlimited mixing were considered, there would be little or no visible plume at the distances used here. Furthermore, simulated photographs using slightly lower wind speeds under the stable conditions would make the plume slightly more apparent.

The cases in which relative humidity is varied are obtained by increasing the size of the individual particles in accordance with Winkler's analysis.[6] This is carried out for background particles and sulfates and nitrates. In these cases the background visual range is altered as the particles absorb water and increase in size. The fly ash is assumed to be insoluble so that no increase in size is expected.

The simulated photographs can be associated with various indices used to characterize visibility impairment. Because of the highly nonuniform character of the plume, the values of some of the indices vary with the viewing direction and (sometimes) the distance from the observer. For example, bscat varies from background values near the observer to peak values in the center of the plume. The changes in chromaticity coordinates, CIEΔE values, meteorological visual range, and blue/red ratio depend upon the viewing direction chosen. For the analysis presented here, the center of the viewing angles is used along with the elevation angle that gives the maximum effect of the plume. In the case of CIE Δ E values, the reference intensity is for the same viewing direction at the horizon. Table A-III shows visibility indices associated with study cases.

In addition to these parameters, two other parameters are reported for each photograph color. These are the plume transmission (TR) in each color and the additional light scattered (IS) by the plume in each color. The latter is reported as a ratio of the scattered light intensity to the original unperturbed intensity.

In the haze cases, the visual ranges for each color and bscat for 550 nm are reported in Table A-IV.

The photographic simulation technique requires an output that can be used to modify the film densities in a manner equivalent to that produced by pollution. In the visibility model, this is accomplished by calculating plume

TABLE A-III

VISIBILITY INDICES ASSOCIATED WITH STUDY CASES

CASE	P/H	CIEΔE	X	Y	B/R	Blue TR/IS	Green TR/IS	Red TR/IS
B-1	0.74	12.0	0.03	0.019	0.69	0.43/0.183	0.63/0.087	.86/0.124
B-2	0.83	7.4	0.013	0.013	0.85	0.63/0.119	0.80/0.05	0.93/0.06
B-3	0.87	5.4	0.004	0.008	0.95	0.82/0.07	0.89/0.03	0.97/0.03
B-4	0.75	11.7	0.031	0.019	0.69	0.42/0.20	0.63/0.07	0.86/0.13
B-5	0.75	11.4	0.030	0.017	0.70	0.41/0.22	0.62/0.10	0.84/0.09
B-6	0.88	3.9	0.004	0.004	0.95	0.21/0.57	0.39/0.32	0.62/0.52
B-7	0.80	11.3	0.033	0.017	0.68	0.35/0.30	0.51/0.18	0.70/0.32
B-8	0.68	15.8	0.045	0.023	0.59	0.33/0.14	0.55/0.09	0.85/0.09
B-9	0.76	17.6	0.037	0.019	0.64	0.43/0.57	0.63/0.64	0.86/0.97
B-10	0.87	4.8	-0.007	0	1.09	0.93/0.02	0.96/0.01	1.00/0.0
B-11	0.70	9.0	0.002	-0.002	0.97	0.66/0.08	0.79/0.06	0.93/0.05
B-12	(Plume below horizon)							
B-13	0.74	10.7	0.0274	0.012	0.72	0.44/0.19	0.64/0.08	0.83/0.12
B-14	1.07	3.3	0.004	0.006	0.95	0.45/0.54	0.65/35	0.89/0.19
B-15	0.92	4.8	0.010	0.010	0.88	0.42/0.42	0.62/21	0.85/0.21

transmission and plume scattering at representative points. With this technique the clean scene brightnesses are multiplied by the plume transmission and added to the plume scattering to obtain new brightnesses that are converted to film densities. It also possible to replace the clean scene brightnesses by calculated values of the brightnesses. However, this technique produces transition difficulties unless it is confined to the sky.

TABLE A-IV

VISIBILITY INDICES ASSOCIATED WITH HAZE SIMULATION

Case	Characterization	Bscat ($\times 40^{-4}$ m^{-1})	Visual Range (km)		
			Blue	Green	Red
H-2	0.6 $\mu g/m^3$; 30% RH	0.157		250	
H-3	5 $\mu g/m^3$ SO^4	0.49	62.	90.	116.
H-4	26 $\mu g/m^3$ SO^4	1.96	17.	22.	23.
H-5	60% RH	0.190	119.	206.	309.
H-6	80% RH	0.324	80.	121.	162.
H-7	26 $\mu g/m^3$; 60% RH	3.01	10.6	13.	15.9

The codes currently require emission rates of nitrogen oxide, fly ash, and sulfur dioxide plus stack parameters such as stack height, stack radius, stack temperature, stack gas velocity, and plant elevation. Size distributions for fly ash, sulfates, and nitrates are also input, but usually can be estimated based on reported values.

The meteorological input parameters required are essentially the same as those needed for air dispersion calculations: stability, mixing heights, wind speed, direction, and ambient temperature. Furthermore, the time of day, day of year, viewing angle, elevation, and location (latitude and longitude) associated with the clean slide are also required. In addition, it would be useful if contrast photometer measurements, turbidity measurements, or nephelometer measurements accompany the slide. These measurements are needed to characterize the background atmosphere. However, if they are not provided, the slide densities themselves probably can be used if there is a dark-colored distant terrain feature in the picture. Ideally, the clean slide should have little cloud cover.

REFERENCES

1. Environmental Protection Agency, "Electric Utility Steam Generating Units Proposed Standards of Performance and Announcement of Public Hearing in Proposed Standards," Federal Register, 43, 184, Tuesday, September 9, 1978, pp. 42154-42183.

2. J. A. Ogren, D. L. Blumenthal, and A. H. Vanderpol, "Oxident Measurements in Western Power Plant Plume," Electric Power Research Institute report EPRI-EA-421, July 1977.

3. Raymond Chuen, Brunswick Corporation, Costa Mesa, California, unpublished data, 1978.

4. R. C. Ragaini and J. M. Ondov, "Trace-Element Emissions From Western U. S. Coal-Fired Power Plants," Lawrence Livermore Laboratory preprint 77569, Rev. 1, October 11, 1976.

5. R. A. McClatchey, R. W. Fenn, J. E. A. Selby J. S. Garing, and F. E. Volz, "Optical Properties of the Atmosphere," Air Force Cambridge Research Laboratories report AFCRL-70-0527 (September 1970).

6. Peter Winkler, "The Growth of Atmospheric Aerosol Particles As a Function of the Relative Humidity; II. an Improved Concept of Mixed Nuclei," Aerosol Science, 4, 373-387 (1973).

APPENDIX B

TECHNICAL DESCRIPTION OF THE LASL VISIBILITY MODEL

Investigators at LASL perceived the need for a model that could predict and measure visibility impacts in 1975. Simplistic models were constructed and used until 1977, when it became clear that an improved model was needed to predict visibility impairment adequately. A more sophisticated model, constructed and put into operation in late 1977, produces photographs as output. The model has been under continued development since late 1977 and the validation case has been run. More validation procedures are planned.

The model software of the LASL visibility model includes several parts. These parts may be grouped into one of two categories. The first category involves image-processing routines. There are two programs in this category. The first alters the digitized image to account for distortions produced by the original film's response to varying levels of light intensity. This code transforms the digitized image into the image that would have been obtained with a film having a gamma* value of 1 over the entire range of densities for each color. The code requires the input of film characteristics appropriate to the picture. These input parameters have been prepared for Kodachrome 25 and for Ektachrome 64.

The second program in this category combines the modified digitized image with the transmission and plume-scattering values provided by the other codes. The transmission and scattering values are provided for an array of 10 elevation angles and 10 azimuth angles in the portion of the picture that includes the area covered by the smoke plume. The code calculates the original brightness, B_{old}, for each point of the picture and then constructs new brightness, B_{new}, based on the relation

$$B_{new} = Tr\ B_{old} + B_{sky'},$$

where Tr is the plume transmission and $B_{sky'}$ is the additional contribution from plume-scattered light. The resulting new brightnesses are converted to

---

*Gamma is the slope of the curve of optical density versus log exposure (Gamma = D/ LogE).

film densities. For points other than those for which the Tr and $B_{sky'}$ values are provided, interpolated values of Tr and $B_{sky'}$ are used.

The second category includes the codes that calculate the transmission and scattered light values. There are four programs included in this set. The first program, LEG1, uses mie theory to calculate the scattering efficiency and unnormalized Legendre coefficients for single particles of specified size. Normally, 24 sizes are used in this program. The program must be run separately for each of the three colors.

I. CALCULATION OF MIE SCATTERING FROM SINGLE PARTICLES

The code LEG1 calculates the scattering efficiency and the Legendre coefficients of the phase function for particles of specified size and index of refraction exposed to light of a specified wavelength. The unnormalized Legendre coefficients are obtained from the expansion of the complex mie amplitudes by repeated use of recurrent relationships between the derivative and the products of Legendre functions.

LEG1 normally is used for 24 particle radii beginning with 0.1 microns and continuing by increments of 0.05 to 1.25 microns.

II. CALCULATION OF BACKGROUND RADIATIVE TRANSFER AND FOURIER-LEGENDRE COEFFICIENTS OF THE PHASE FUNCTION

The program NRADT solves the radiative transfers equation for sunlight incident on an atmosphere composed of 30 plane parallel layers. Each layer is assumed homogeneous, and only Rayleigh and mie scattering are considered.

The initial step in the solution is the expansion of the mie and Rayleigh phase function in Fourier-Legendre coefficient

$$M(\mu,\phi;\mu^1,\phi^1) = \sum_{n=1}^{N} F_n^{(m)} (\mu,\mu^1) \cos[(n-1)(\phi^1 - \phi)]$$

and

$$R(\mu,\phi,\mu^1,\phi^1) = \sum_{n=1}^{3} F_n^{(r)} (\mu,\mu^1) \cos[(n-1)(\phi^1 - \phi)],$$

$$F_m^{(m)}(\mu,\mu^1) = (2 - \delta_{o,m-1}) \sum_{i=m-1}^{N} \Lambda_{i+1}^{(m)} \frac{(i-m+1)!}{(i+m-1)!} P_i^{m-1}(\mu) P_i^{m-1}(\mu^1)$$

and

$$F_m^{(r)}(\mu^1,\mu^1) = (2 - \delta_{o,m-1}) \sum_{i=m-1}^{3} \Lambda_{i+1}^{(r)} \frac{(i-m+1)!}{(i+m-1)!} P_i^{m-1}(\mu) P_i^{m-1}(\mu^1) .$$

The radiative transfer equation for a semi-infinite plane parallel atmosphere is

$$\mu \frac{dI(\tau;\mu,\phi)}{d\tau} = I(\tau;\mu,\phi) - w(\tau) J(\tau;\mu,\phi) ,$$

where $I(\tau;\mu,\phi)$ is the intensity of radiation emerging at a level in the atmosphere corresponding to a normal optical thickness τ in the direction μ,ϕ, and μ is $\cos\theta$; θ is the angle the propagation direction makes with the local zenith; ϕ is the azimuth angle referred to an arbitrary meridian plane. The $W(\tau)$ is the albedo of single scattering, given by

$$w(\tau) = [\Delta\tau^{(s,m)} + \Delta\tau^{(s,r)}] / \Delta\tau ,$$

where $\Delta\tau^{(s,m)}$ refers to the change in optical depth in traversing unit volume associated with mie scattering and $\Delta\tau(s,r)$ is the change in optical depth in traversing unit volume associated with Rayleigh scattering. The source term $J(\tau;\mu,\sigma)$ is given by

$$J(\tau;\mu,\phi) = \frac{1}{4\pi} e^{-\tau/\mu_o} P(\tau;\mu,\phi;-\mu_o,\phi_o)F + \frac{1}{4\pi} \int_{-1}^{+1} \int_{0}^{2\pi} P(\tau;\mu,\phi;\mu^1,\phi^1)I(\mu^1,\phi^1)d\mu^1 d\phi^1 ,$$

where it is assumed that F is the solar radiation flux per unit area of $\tau = o$ at right angles to the incident direction represented by $-\mu_o, \phi_o$. The boundary conditions are

$$I(0; -\mu,\phi) = 0$$

and

$$I(\tau_b; +\mu,\phi) = 0.$$

The contribution from ground reflection is treated separately through a technique developed by Chrondrasekhor.[1] In the technique, an amount $I^{*(1)}(\tau i; \pm \mu)$ is added to the calculated intensity $I,^{(m)}(\tau i; \pm \mu)$. The $I^{*(1)}(\tau; \pm \mu)$ is chosen to so that the solution $I,^{(n)}(\tau i; \pm \mu) + I^{*(1)}(\tau i; \pm \mu)$ satisfies the relation

$$A = \frac{2\pi \int_o^1 I^{*(1)}(\tau_b;+1)\mu d\mu}{\mu_o F e^{-\tau_b}/\mu_o + 2\pi \int_{-1}^{o} [I_1^{(m)}(\tau_b;-\mu) + I^{*,(1)}(\tau_b; -\mu)]\mu d\mu}.$$

The solution technique involves expansion of the intensities in the form

$$I(\tau,\mu,\phi) = \sum_{n=o}^{N} I_n(\tau,\mu) \cos n\phi,$$

where the subscript j refers to the τ dependence and k refers to the de-pendence. The source terms are similarly expanded. The resulting equations are solved by an iteration technique.[2] In the iterative technique, the first approximation to the source term $J(\tau;\mu,\phi)$ is taken as the direct sunlight term

$$J_m^{(1)}(\tau_i;\mu) = \frac{1}{4\pi} F_e^{-\tau i/\mu_o} P_m(\tau_i; \mu, -\mu_o).$$

where

$$P_m(\tau_i;\mu, -\mu_o) = T(\tau_i)\, F_m^{(m)}(\mu,-\mu_o) + [1 - T(\tau_i)]\, F_m^{(r)}(\mu, -\mu_o).$$

This value for the source term permits the calculation of diffuse intensities for each layer. The resulting intensities are substituted into the source term, and new intensities are calculated. This procedure continues until the differences between succeeding values of the intensities are negligible.

III. CALCULATION OF PLUME DISPERSION AND PLUME RADIATIVE TRANSFER

The program NPVIS computes the dispersion of the pollutants and the radiative transfer associated with the pollutant cloud. Plume dispersion begins with plume rise from the stack which is calculated by the Briggs procedure. Plume dispersion is given by a gaussian formulation

$$X(x,y,z,H) = \frac{Qe^{-\frac{1}{2}\left(\frac{y}{\sigma_y}\right)^2}}{2\,\bar{u}\,\sigma_y\,\sigma_z\,\pi} \left\{ e^{-\frac{1}{2}\left(\frac{H-z}{\sigma_z}\right)^2} + e^{-\frac{1}{2}\left(\frac{H+z}{\sigma_z}\right)^2} \right\},$$

where H is the effective plume bright, μ is the wind speed, Q is the effective emission rate, σ_y is the horizontal dispersion parameter, and σ_z is the vertical dispersion parameter. The effective plume height is merely

$$H = Hs + \Delta H,$$

where Hs is the stack height and ΔH is the plume rise.

In cases where there is a mixing layer above ground, a series formulation is used to account for multiple reflection between the ground and the elevated stable layer.

It is necessary to use an effective emission rate because some of the most important visible pollutants are transformed from invisible ones. For example, the effective emission rate for particulate sulfate is obtained from the relation

$$Q\ \text{sulfate} = QSO_2\ \text{mcf} \left[1 - e^{\left(\frac{-0.693\ x}{ut_{1/2}}\right)}\right],$$

where QSO_2 is the sulfur dioxide emission rate, mcf is the ratio of the mass of a sulfate molecule to that of a sulfur dioxide molecule, x is the downwind distance, u is the wind speed and $t_{1/2}$ the conversion half-life. The conversion half-life is found from photochemical model prediction or field experience.

Once the concentration is known, the extinction coefficient per unit volume and the scattering coefficient per unit volume can be found.

The first step in computing the plume radiation transfer is to choose several lines of sight that are representative of the view seen by an observer. For each line of sight, a numerical integration of the extinction coefficient per unit volume and the scattering coefficient per unit volume is carried out to give the total optical depth and the scattering optical depth. The total change in optical depth is then represented by a series of infinite slabs specified by a change in optical depth and a change in scattering optical depth.

Once the slabs have been obtained, the radiation transfer is calculated in a fashion similar to that for a uniform atmosphere. In this case the boundary conditions are

$$I(o; -\mu_1) = Io(\tau_b; -\mu_1)$$

and

$$I(\tau \max; +\mu_1) = Io(\tau_b; \mu_1)$$

where $Io(\tau_b;\mu_1)$ and $Io(\tau_b; -\mu_1)$ are the background light intensities derived from coordinate transformations from the solutions found by NRADT. The iterative technique involves starting at the outermost slab using the boundary conditions for $I(o, -\mu_1)$ and marching inward until the last slab is reached. Then the innermost boundary condition is used and the marching proceeds outward until the outermost slab is reached. The procedure continues until the system converges.

The solution to the radiation transfer equation allows one to calculate both the light transmitted unaltered by the plume and the additional light scattered into the line of sight by the plume. From this information new equivalent film densities can be calculated as

$$D_{new} = \gamma \log \left[A \left(\frac{Tr}{A} \, 10^{\frac{-D_o}{\gamma}} + B_{sky} \right) \right],$$

where γ refers to the gamma of the film and D_o is the old film density. The constant A is found by comparing the background calculated intensity to the film density of the original slide as

$$A = \frac{10^{\frac{-D_{ref}}{\gamma}}}{I_{ref}},$$

where I_{ref} refers to the calculated intensity corresponding to the point at which the film density D_{ref} is measured. There will be different values of D_{ref}, I_{ref}, and A for each color.

Several approximations used in MNRADT may affect the final output. First, light intensities and phase functions are calculated for only 20 values of the cosine of the angle of propagation with the local zenith. Second, the calculations are made for a plane parallel atmosphere rather than for concentric spherical shells. Third, only a limited number of Fourier coefficients are carried. Fourth, the ground is assumed to have uniform albedo, and the sky is assumed to be cloudless. Finally, the output of the code is sensitive to the input parameters used.

NPVIS also uses several approximations. The calculated air dispersion may involve significant uncertainties although the integration across the plume tends to reduce the uncertainties somewhat. In this context, no allowance is made for dry deposition, which would be important for neutral or unstable conditions at large downwind distances. Also, the model does not treat complexities in the wind flow patterns produced by terrain features. Furthermore, the reaction rates and chemistry used are highly simplified. Important possible errors include the manner in which nitrogen dioxide is formed from nitric oxide and the failure to provide for destruction of nitrogen dioxide by hydroxyl ions. Furthermore, an important oversimplification is the lack of description of changes in particle size distribution as the plume drifts downwind.

The radiative transfer description suffers from many of the same difficulties of MNRADT, although the restriction to few Fourier coefficients is

appropriate in this case. Major approximations include the use of semi-infinite planes to represent the finite pollution clouds and the neglect of changes in incident sunlight produced by the pollution cloud. There is also some uncertainty associated with the fact that calculations are usually made for a limited number of elevation angles and azimuth angles (usually 10 or 15 elevation angles and 10 or 15 azimuth angles). The calculated values are then interpolated over the entire picture.

In general, the LASL visibility model is quite flexible. The limited validation done to date has been encouraging; however, there remain significant uncertainties, which have been discussed.

REFERENCES

1. S. Chandrasekhar, Radiative Transfer (Dover Publications, Inc., New York, 1960).

2. Norman Braslau and J. V. Dave, "Effect of Aerosols on the Transfer of Solar Energy Through Realistic Model Atmospheres," IBM Research Report RC4114, Palo Alto, California 1972.

☆ U.S. Government Printing Office: 1979 — 677—115/217

Printed in the United States of America. Available from
National Technical Information Service
US Department of Commerce
5285 Port Royal Road
Springfield, VA 22161

Microfiche $3.00

001-025	4.00	126-150	7.25	251-275	10.75	376-400	13.00	501-525	15.25
026-050	4.50	151-175	8.00	276-300	11.00	401-425	13.25	526-550	15.50
051-075	5.25	176-200	9.00	301-325	11.75	426-450	14.00	551-575	16.25
076-100	6.00	201-225	9.25	326-350	12.00	451-475	14.50	576-600	16.50
101-125	6.50	226-250	9.50	351-375	12.50	476-500	15.00	601-up	

Note: Add $2.50 for each additional 100-page increment from 601 pages up.